Inorganic Chemistry

Article

pubs.acs.org/IC

Unsymmetrical Chelation of N-Thioether-Functionalized Bis(diphenylphosphino)amine-Type Ligands and Substituent Effects on the Nuclearity of Iron(II) Complexes: Structures, Magnetism, and Bonding

Christophe Fliedel,[†,▽] Vitor Rosa,[†,▽] Andrés Falceto,[§] Patrick Rosa,[‡] Santiago Alvarez,*[,§] and Pierre Braunstein*[,†]

[†]Laboratoire de Chimie de Coordination, Institut de Chimie, UMR 7177 CNRS, Université de Strasbourg, 4 rue Blaise Pascal, 67081 Strasbourg Cedex, France

[‡]CNRS, Université de Bordeaux, ICMCB (UPR 9048), 87 avenue du Dr. A. Schweitzer, 33600 Pessac, France

[§]Departament de Química Inorgànica and Institut de Química Teòrica i Computacional, Universitat de Barcelona, Martí i Franquès 1-11, 08028 Barcelona, Spain

Supporting Information

ABSTRACT: Starting from the short-bite ligands N-thioether-functionalized bis(diphenylphosphino)amine-type $(Ph_2P)_2N(CH_2)_3SMe$ (**1**) and $(Ph_2P)_2N(p\text{-}C_6H_4)SMe$ (**2**), the Fe(II) complexes $[FeCl2(\mathbf{1})]_n$ (**3**), $[FeCl_2(\mathbf{2})]_2$ (**4**), $[Fe(OAc)(\mathbf{1})_2]PF_6$ (**5**), and $[Fe(OAc)(\mathbf{2})_2]PF_6$ (**6**) were synthesized and characterized by Fourier transform IR, mass spectrometry, elemental analysis, and also by X-ray diffraction for **3**, **4**, and **6**. Complex **3** is a coordination polymer in which **1** acts as a *P*,*P*-pseudochelate and a (*P*,*P*),*S*-bridge, whereas **4** has a chlorido-bridged dinuclear structure in which **2** acts only as a *P*,*P*-pseudochelate. Since these complexes were obtained under strictly similar synthetic and crystallization conditions, these unexpected differences were ascribed to the different spacer between the nitrogen atom and the −SMe group. In both compounds, one Fe−P bond was found to be unusually long, and a theoretical analysis was performed to unravel the electronic or steric reasons for this difference. Density functional theory calculations were performed for a set of complexes of general formula $[FeCl_2(SR_2)\{R^1_2PN(R^2)P'R^3_2\}]$ (R = H, Me; R^1, R^2, and R^3 = H, Me, Ph), to understand the reasons for the significant deviation of the iron coordination sphere away from tetrahedral as well as from trigonal bipyramidal and the varying degree of unsymmetry of the two Fe−P bonds involving pseudochelating PN(R)P ligands. Electronic factors nicely explain the observed structures, and steric reasons were further ruled out by the structural analysis in the solid-state of the bis-chelated complex **6**, which displays usual and equivalent Fe−P bond lengths. Magnetic susceptibility studies were performed to examine how the structural differences between **3** and **4** would affect the interactions between the iron centers, and it was concluded that **3** behaves as an isolated high-spin Fe(II) mononuclear complex, while significant intra- and intermolecular ferromagnetic interactions were evidenced for **4** at low temperatures. Complexes **3** and **4** were also tested in catalytic ethylene oligomerization but did not exhibit any significant activity under the studied conditions.

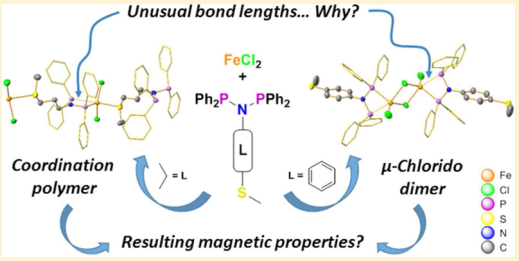

INTRODUCTION

The fine-tuning of the structure, reactivity, and electronic and catalytic properties of metal complexes through a judicious choice of ligands represents a central aspect of coordination chemistry and explains why short-bite ligands such as bis(diphenylphosphino)amine (DPPA, Chart 1) and its N-substituted (when the substituent contains only C and H atoms) or N-functionalized (when an additional donor function or a metal is linked to the central N atom) analogues (Chart 1) have attracted continuing interest over the past 20 years. Their diverse applications in coordination chemistry and homogeneous and heterogeneous catalysis have been reviewed.[1,2] In addition to the versatility of their coordination modes (i.e., monodentate, bridging, or chelating) typical of numerous short-bite ligands, mainly explored with bis(diphenylphosphino)-methane (DPPM) and DPPA (Chart 1), N-substitution in the latter, which is easier than C-substitution in DPPM, allows the introduction of a large variety of groups that offer one or more additional donor functions, thus broadening the scope of structural motifs accessible in their coordination compounds.

Taking advantage of these possibilities, a large diversity of mono- or polynuclear coordination complexes have been isolated. Our group has previously reported the synthesis of mono-, di-, and tetranuclear or higher nuclearity metal complexes or clusters, involving binding to the metal(s) of

Received: April 17, 2015
Published: June 23, 2015

DOI: 10.1021/acs.inorgchem.5b00834
Inorg. Chem. 2015, 54, 6547−6559

Chart 1. DPPM and DPPA Short-Bite Ligands and the N-Substituted[a] and N-Functionalized[b] Derivatives of the DPPA Ligand

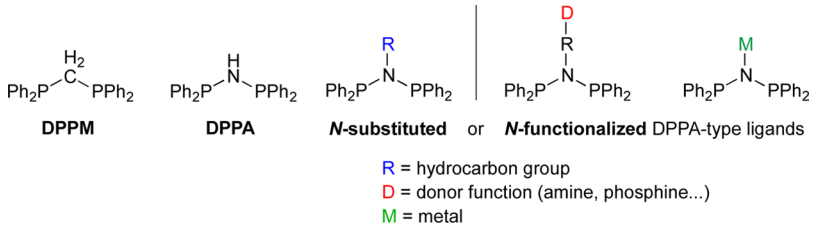

[a]Only C- and H-containing group. [b]If an additional donor function or a metal is linked to the central N atom.

Scheme 1. Synthesis of the Fe(II) Complexes 3 and 4[a]

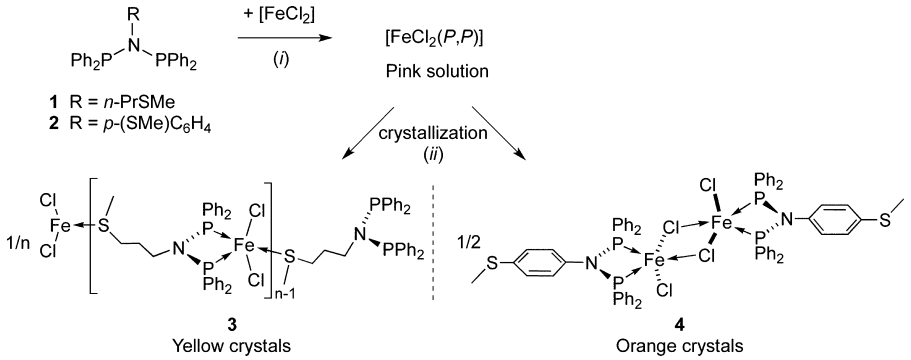

[a]Conditions: (i) CH_2Cl_2, room temperature, 12 h; (ii) reduction of the original reaction volume to one-third followed by layering with pentane.

both phosphine donors, with or without the participation of the N-substituent.[3] Incorporation of an alkoxysilyl or a thioether group in the N-substituent has allowed the anchoring of metal complexes into mesoporous matrices[4] or on the gold surface of Janus microspheres, respectively.[5]

Chromium(III) complexes of such PN(R)P ligands remain extensively studied in catalytic ethylene oligomerization owing to their exceptional ability to produce selectively (1-)hexene and/or (1-)octene when employed as precatalysts in combination with aluminum-based cocatalysts.[6,7] Nickel(II) halide complexes containing DPPA-type ligands are also interesting candidates for ethylene oligomerization,[7e,8] while their palladium(II) analogues were successfully used in catalytic coupling reactions.[9] Very recently, a combination of dicationic Ni(II) complexes, in which the metal center is bis-chelated by two N-thioether-functionalized DPPA-type ligands, and Zn metal was found to readily perform the activation of C_{sp3}–Cl bonds under mild conditions and afford mixed phosphine-phosphonium ylide species.[10]

Since iron is an earth-abundant, cheap, and nontoxic metal,[11] its coordination complexes have recently attracted increasing attention as alternatives to precious metal complexes in homogeneous catalysis.[12] Among the various catalytic applications of iron complexes, we note the catalytic oligomerization of ethylene[13,14] and the atom-transfer or organometallic-mediated radical polymerization (ATRP and OMRP, respectively).[15] Low-coordinated and/or ligand-constrained geometry Fe(I or II) complexes have also been studied over the past five years because of their possible behavior as single-molecule magnets (SMM).[16] Interestingly, only very few examples of Fe complexes coordinated by DPPA-type ligands, whether N-substituted by a hydrocarbon chain or another donor function, have been structurally characterized,[17] and most of them were studied as models of the iron-only [FeFe] hydrogenase.[18] These considerations prompted us to study the possible formation of iron(II) complexes from $FeCl_2$ and ligands **1** and **2** (Scheme 1), since the resulting coordination complexes could be of potential interest in molecular magnetism and/or catalysis. For example, the presence of the additional thioether group in the N-substituent could result in (i) intermolecular interactions of interest for electronic communication between metal centers, (ii) the stabilization of catalytically active, electron-deficient species, including through hemilability,[19] and/or in favorable interactions with a cocatalyst, (iii) controlled anchoring of molecules on metal surfaces.[5,20] In this study, we detail the synthesis and characterization of complexes obtained by reaction of ligands **1** and **2** with $FeCl_2$ and show that, while the structures of the ligands are very similar, their complexes, **3** and **4**, respectively, exhibit considerable differences. Although in both cases an unsymmetrical coordination of the phosphorus atoms led to pseudochelation of their respective ligands, **3** is a coordination polymer, whereas **4** is a dinuclear complex. The more encumbered bis-chelated $[Fe(OAc)(P,P)_2]PF_6$ complexes (**5**, **6**) were also synthesized to determine experimentally whether steric factors could be responsible for this uncommon M–P bonding.

RESULTS AND DISCUSSION

Synthesis and Structural Characterization. With the aim to synthesize complexes of the type $[FeCl_2(P,P)]$ (*P*,*P* = ligand **1** or **2** in a chelating mode) and evaluate the influence of the nature of the thioether donor function (i.e., with a propylene vs a para-substituted phenylene spacer) on the resulting complexes, we reacted solid anhydrous $FeCl_2$ with a dichloromethane solution of ligand **1** or **2**, in a 1:1 metal/ligand ratio under inert atmosphere. After filtration, concentration of the light pink reaction mixture and crystallization by slow diffusion of pentane, yellow $[FeCl_2(\mathbf{1})]$ (**3**) and orange $[FeCl_2(\mathbf{2})]$ (**4**) crystals were isolated in nearly quantitative

DOI: 10.1021/acs.inorgchem.5b00834
Inorg. Chem. 2015, 54, 6547–6559

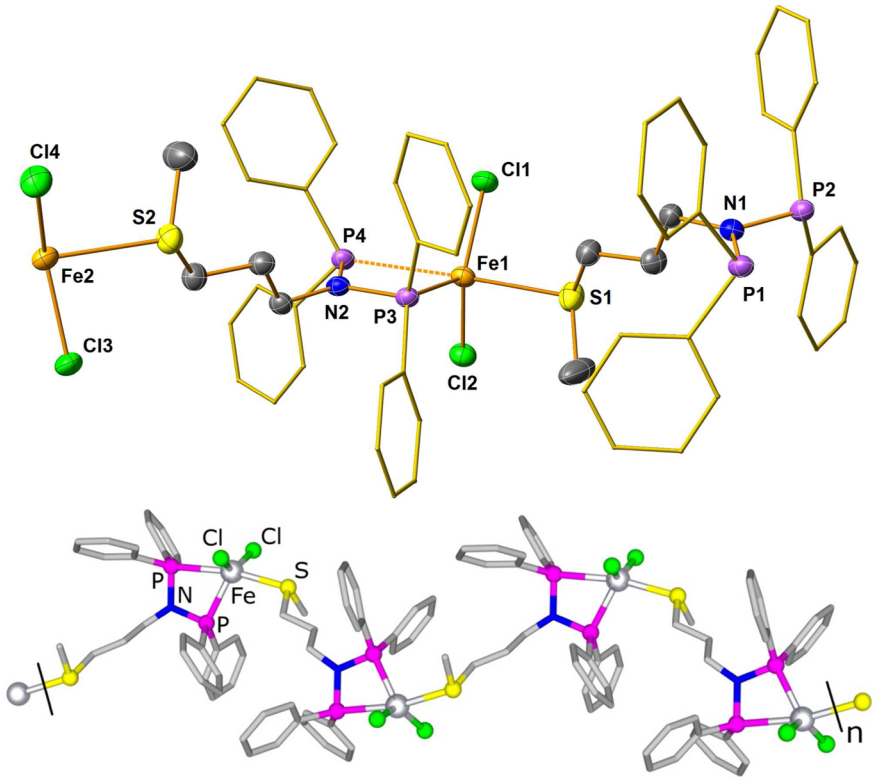

Figure 1. (upper) View of the molecular structure of the asymmetric unit of **3**. Hydrogen atoms were omitted, and P-phenyl substituents are represented in stick style for clarity. Ellipsoids represented at 50% probability level. (lower) Simplified view of **3** illustrating the zigzag conformation of the coordination polymer. The H atoms are omitted for clarity. Selected bond distances and angles are summarized in Table 1.

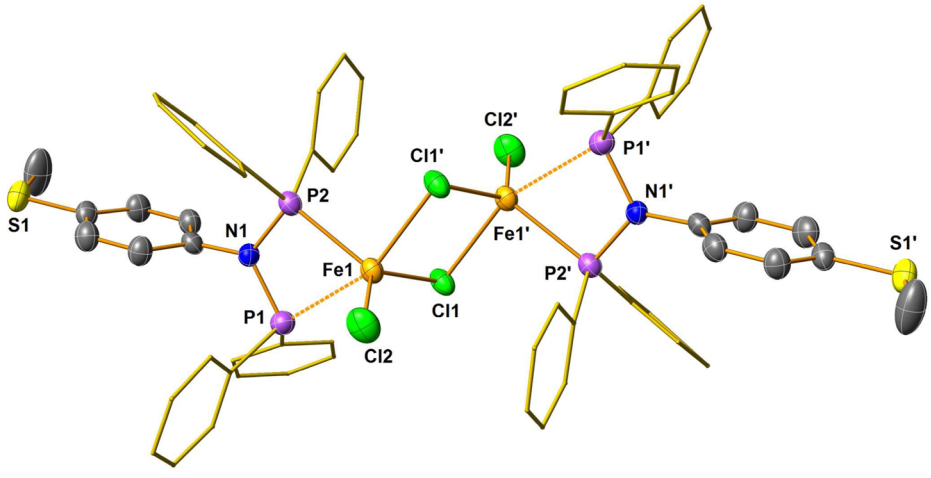

Figure 2. View of the molecular structure of **4**. Hydrogen atoms were omitted, and P-phenyl substituents are represented in stick style for clarity. Ellipsoids are represented at 50% probability level. Selected bond distances and angles are summarized in Table 1.

yields, respectively (Scheme 1). Because of their paramagnetic nature, these complexes could not be analyzed by NMR spectroscopy, and thus their structure in solution was not unambiguously established. However, they were characterized by Fourier tranform infrared (FT-IR), mass spectrometry (MS), and elemental analysis, and their molecular solid-state structure was determined by X-ray diffraction analysis.

Once formed, the yellow crystals of **3** could not be redissolved in dichloromethane, which is consistent with the polymeric nature of this complex unambiguously established by single-crystal X-ray diffraction studies (Figure 1). In the case of ligand **2** with a more rigid phenylene spacer, under experimental conditions otherwise completely similar, formation of a chlorido-bridged dinuclear complex **4**, instead of a coordination polymer (Figure 2 vs Figure 1), could result from a combination of electronic, steric, or solubility factors, but the former will be shown by density functional theory (DFT) calculations to be dominant (see below). Selected bond lengths and angles in the two structures are given in Table 1. The differences between **3** and **4** emphasize how relatively small changes in the ligand architecture, that is, the nature of the spacer between the PNP chelate and the thioether function, can critically affect the structure of the resulting metal complexes. In the present case, the formation of a coordination polymer or

DOI: 10.1021/acs.inorgchem.5b00834
Inorg. Chem. 2015, 54, 6547−6559

Table 1. Selected Bond Lengths (Å) and Angles (deg) for 3, 4, and 6

	3	4	6		3		4		6
Fe1−P1		2.762(1)	2.236(1)	P3−Fe1−P4	64.55(5)	P1−Fe1−P2	64.98(3)	P1−Fe1−P2	71.68(4)
Fe1−P2		2.465(9)	2.217(1)					P3−Fe1−P4	71.65(4)
Fe1−P3	2.457(2)		2.223(1)	P3−Fe1−Cl1	110.9(7)	P2−Fe1−Cl2	119.1(4)	P1−Fe1−O1	88.50(9)
Fe1−P4	2.798(2)		2.219(1)	P3−Fe1−Cl2	109.8(6)	P2−Fe1−Cl1	113.1(3)	P4−Fe1−O2	90.92(9)
Fe1−Cl1	2.252(2)	2.339(9)						O1−Fe1−O2	64.4(1)
Fe1−Cl2	2.258(2)	2.221(1)		P3−Fe1−S1	104.3(6)	P2−Fe1−Cl1′	92.89(3)	P2−Fe1−O1	97.47(9)
Fe1−S1	2.580(2)			P4−Fe1−S1	168.8(6)	P1−Fe1−Cl1′	156.5(3)	P3−Fe1−O2	93.66(9)
Fe1−Cl1′		2.515(9)						P2−Fe1−P3	107.2(5)
Fe1−O1			2.027(3)	P3−N2−P4	111.7(3)	P2−N1−P1	111.0(1)	P1−N1−P2	98.3(2)
Fe1−O2			2.034(3)					P3−N2−P4	98.2(2)

of a chlorido-bridged dimer may suggest different physical and chemical properties for these complexes, as will be shown below with their magnetic behavior. Langer et al. recently studied the reactivity of $FeCl_2$ toward 1,2-bis-(diphenylphosphanyl)ethane (DPPE) and 1,2-bis-(diisopropylphosphanyl)ethane and highlighted a high lability of the diphosphine ligands, which were found to behave as bridging or chelating ligands in the former case but solely as chelating ligands in the latter.[21]

The electrospray ionization mass spectrometry (ESI-MS) spectrum of complex **3** could be recorded when the compound was dissolved in a coordinating solvent (MeCN), and it exhibits a major peak for the $[FeCl(\mathbf{1})_2]^+$ fragment (m/z = 1037.2). In contrast, the major peak in the spectrum of complex **4** corresponds to a much smaller fragment (m/z = 598.0 $[FeCl(\mathbf{2})]^+$ or $[M\text{-}2Cl]^{2+}$); however, the $[M\text{-}Cl]^+$ and $[M+Na]^+$ fragments (m/z = 1233.0 and 1291.6, respectively) were also detected. Elemental analyses performed on crushed samples of the crystalline material were in agreement with the $[FeCl_2(P,P)]$ (P,P = **1** or **2**) stoichiometry (see Experimental Section).

The molecular structure of complex **3** revealed a distorted trigonal bipyramidal coordination sphere for the iron(II) center, composed of two phosphorus atoms from one pseudochelating ligand **1** (see below), two chlorido ligands and the sulfur atom of a second ligand **1**, which results in a one-dimensional coordination polymer of a zigzag conformation (Figure 1).

The equatorial plane of the trigonal bipyramid contains the atoms P3, Cl1, and Cl2, and the Fe−P3 bond [2.457(2) Å] is significantly longer than the Fe−Cl bonds [2.253(2) (Cl1) and 2.258(2) (Cl2) Å]. The longest metal−ligand bonds involve the apical ligands, with Fe1−P4 and Fe1−S1 bond lengths of 2.798(2) and 2.580(2) Å, respectively. The unusually long Fe1···P4 distance leads to the description of the diphosphine ligand as pseudochelate, and there is no obvious steric or electronic reason that could explain it; that is, there is no bulky group linked to the metal or a donor group in trans position to P4 with a strong trans-influence (see below the Theoretical Calculations Section). The value of the distance between P4 and Fe1 is between that for a dative bond (2.10−2.52 Å, see Supporting Information, Figure S1) and a Fe···P short contact (3.0−5.0 Å, see Supporting Information, Figure S2). The most significant distortion away from regular trigonal bipyramidal geometry is imposed by the bite angle of the ligand [P3−Fe1−P4 = 64.55(5)°]. Important parameters for the magnetic properties (see below) are intra- and intermolecular distances between the iron centers, Fe1···Fe2 = 10.352(1) Å and Fe1···Fe1 = 9.106(1) Å. The Fe−Fe−Fe angle along one polymeric chain is 109.37(1)°. A related iron(II) coordination polymer with a zigzag chain structure assembled by nitrogen-containing ligands revealed an interesting spin-crossover (high-spin/low-spin transition) as a function of temperature.[22]

Figure 1(lower) shows a simplified view of the solid-state arrangement of complex **3** and highlights the zigzag arrangement of the coordination polymer resulting from the assembling of $FeCl_2$ units through ligand **1**, which acts as a κ^2-*P,P*-chelating (Fe1) and as a κ^2-(*P,P*),*S*-bridging (Fe1−Fe2) ligand via the diphosphine and the thioether functions.

An X-ray diffraction analysis on single crystals of complex **4** revealed a centrosymmetric molecular structure in the solid state, with the iron(II) center in a distorted trigonal bipyramidal coordination environment, as in complex **3** (Figure 2). However, in contrast to **3**, the coordination sphere of the metal in **4** is composed of one *P,P*-pseudochelating ligand **2**, one terminal chlorido, and two μ_2-bridging chlorido ligands. The trigonal plane contains the atoms P2, Cl1, and Cl2, with Fe1−P2 [2.465(9) Å] being significantly longer than the iron chloride bonds [2.339(9) (Cl1) and 2.221(1) (Cl2) Å]. The apical positions of the bipyramid are occupied by P1 and Cl1′. While the Fe−Cl bond lengths involving the bridging atoms Cl1 and Cl1′, of 2.339(9) and 2.515(9) Å, respectively, are in the range found in other chlorido-bridged, phosphine iron(II) dinuclear complexes [2.358(3)−2.5815(4) Å],[23] the Fe1···P1 distance of 2.762(1) Å is unusual. It is shorter than the corresponding distance in complex **3** (Table 1) but remains between those typical for a coordination bond and a short contact (see Supporting Information, Figures S1 and S2). Although the metal centers in complexes **3** and **4** have a similar coordination geometry and are supported by the same class of ligands (**1**, **2**), most of their characteristic structural parameters differ significantly, and the only bond lengths and angles they have in common are those directly involving the chelating short-bite ligands, that is, the Fe−P bonds and the P−Fe−P and P−N−P angles (Table 1). In contrast, significant differences are observed between the P−Fe−S and P−Fe−Cl1$^{(\prime)}$ angles, and the Fe−S and Fe−Cl1$^{(\prime)}$ bond lengths. Owing to the different nature of the spacer between the PNP moiety and the S donor in **1** and **2**, the Fe1···Fe1′ distance in **4** [3.540(7) Å] is much shorter than the Fe1···Fe2 [10.352(1) Å] and Fe1···Fe1 [9.106(1) Å] separations in **3**. Intermolecular distances are also quite short, with the shortest separation being Fe1···Fe1 = 8.926(8) Å.

A comparison between **3** and **4** illustrates the major influence of the nature of the spacer connecting the two sets of donor groups in polyfunctional ligands on the nature and structure of their metal complexes. Under similar reaction conditions, a flexible aliphatic spacer between the diphosphine and the

DOI: 10.1021/acs.inorgchem.5b00834
Inorg. Chem. 2015, 54, 6547−6559

thioether groups leads to a polymeric assembly involving a bridging bonding mode for the polyfunctional ligand, whereas with a rigid aromatic spacer, a chlorido-bridged dinuclear complex was formed, and no intermolecular interaction was observed with the thioether function.

To examine whether in addition to electronic factors, steric factors should also be invoked to explain the long Fe−P distances in complexes **3** and **4**, we attempted the synthesis of bis-chelated Fe(II) complexes with ligands **1** and **2**, of general formula $[Fe(X)_2(P,P)_2]$ or $[Fe(X)(P,P)_2]X'$ (X and X′ = anionic ligand, for example, halide, acetate, PF_6; *P*,*P* = **1**, **2**). Such compounds should present a more saturated metal coordination sphere, thus preventing the occurrence of short intermolecular Fe···Fe contacts. Combined with the computational results, a comparative structural analysis should lead to a better understanding of these unusual bond lengths (see below).

The isolated powders resulting from the reaction of ligand **1** or **2** with anhydrous $FeCl_2$, in a 2:1 ligand/metal ratio, in the presence of $LiPF_6$ or not, did not lead to satisfactory analytical data. However, when 2 equiv of **1** or **2** were reacted in dichloromethane at room temperature for 12 h with 1 equiv of $Fe(OAc)_2$ in the presence of excess $LiPF_6$, orange-red solids were isolated by filtration, and their analytical data corresponded to $[Fe(OAc)(P,P)_2]PF_6$ (see Experimental Section). In particular, a peak at m/z = 1061.25 and 1129.21 with the expected isotopic distribution was recorded in the ESI-MS spectra of **5** and **6**, respectively, corresponding in both cases to the $[M\text{-}PF_6]^+$ fragment. Red single crystals of **6**, suitable for X-ray diffraction studies, were obtained by slow diffusion of pentane into a saturated solution of **6** in dichloromethane (Figure 3).

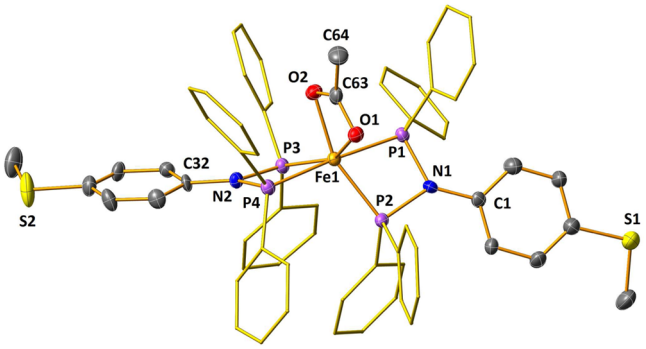

Figure 3. View of the molecular structure of **6**. The PF_6 anion and the hydrogen atoms are omitted, and the P-phenyl substituents are represented in stick style for clarity. Ellipsoids are represented at 50% probability level. Selected bond distances and angles are summarized in Table 1.

The analysis of the molecular structure of **6** confirmed the presence of a hexacoordinated Fe(II) center in a distorted octahedral coordination environment, in which the base is composed by the acetate ligand and two phosphorus atoms (P2, P3) of two different ligands **2**, and the apical positions of the octahedron are occupied by the other two P atoms (P1, P4). The main deviations from regular octahedral geometry are caused by the chelating ligands since the O1−Fe1−O2, P1−Fe1−P2, and P3−Fe1−P4 angles are 64.4(1), 71.68(4), and 71.65(4)°, respectively, instead of 90°. The P2−Fe1−P3 angle of 107.2(5)° is much larger than the expected 90°. An important result from the analysis of this solid-state structure is

Scheme 2. Synthesis of the Fe(II) Complexes 5 and 6[a]

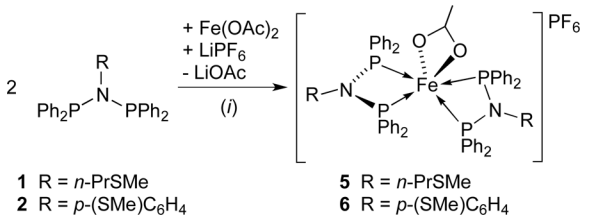

1 R = *n*-PrSMe
2 R = *p*-(SMe)C_6H_4
5 R = *n*-PrSMe
6 R = *p*-(SMe)C_6H_4

[a]Conditions: (i) CH_2Cl_2, room temperature, 12 h. Note: the proposed arrangement of the ligands is based on the X-ray structure analysis of complex **6** (see Figure 3) and the similarity of the FT-IR and ESI-MS spectra of complexes **5** and **6**.

that the Fe−P elongation observed in complexes **3** and **4** is not due to steric reasons, since despite an arrangement around the Fe center in **6** much more sterically encumbered, all the Fe−P bond lengths are nearly equivalent and in the "normal" range (2.217(1)−2.236(1) Å, Table 1). Therefore, electronic reasons should be invoked to elucidate/rationalize the factors responsible for the unusual structural features observed in **3** and **4**, and theoretical calculations were performed (see following section).

Theoretical Calculations. Whereas the two P−metal bond distances of the chelate ring are usually similar in DPPA-type complexes, the very different P−Fe distances found in **3** and **4** and the resulting unusual metal coordination geometries prompted a theoretical analysis of the bonding in these complexes. Let us consider first these compounds as containing a *P*,*P*-chelated metal center and try to analyze later the unusual lengthening of one of the metal−phosphorus bonds. In general, high-spin d^6 tetracoordinated complexes are expected to have a tetrahedral geometry with four σ-donor ligands and nearly tetrahedral with four π-donor ligands.[24] However, a model compound with a mixed ligands set, $[Fe(NH_3)_2Cl_2]$, has the geometry of flattened tetrahedron (42% along the pathway from the tetrahedron to the planar square).[25] Upon incorporation of an additional ammonia ligand to the coordination sphere of this model complex, the resulting pentacoordinate $[Fe(NH_3)_3Cl_2]$ complex adopts practically a square pyramidal geometry; that is, the initial FeN_2Cl_2 *core* goes now all the way to a nearly square planar arrangement. Another consequence of the association of the fifth ligand is an elongation of the Fe−Cl distances from 2.25 to 2.32 Å and of the Fe−N distances from 2.17 to 2.26 Å.

Let us move now to a model closer to our experimental system but replacing the bis(diphenylphosphino)amine with a monodentate analogue and incorporating a simplified version of the thioether, in $[FeCl_2(SMe_2)(Ph_2PNMe_2)]$ (last entry in Table 2). This complex with two σ-donor and two π-donor ligands appears also as a flattened tetrahedron, as in our previous simpler model, but now only at 24% along the path to the square. If we then incorporate the N-methyl-substituted bis(diphenylphosphino)amine ligand in $[FeCl_2(SMe_2)\{Ph_2PN(Me)PPh_2\}]$, we observe a weak coordination of the second phosphorus donor, with an Fe−P distance of 2.70 Å, much longer than that for the fully coordinated phosphorus (2.43 Å) and in good agreement with the two experimental values found in the structures of **3** and **4** (2.76 and 2.80 Å).

To unravel the reasons for such an unsymmetric bonding situation, we start by optimizing a highly simplified model of complex **3** in which all substituents are replaced by hydrogen atoms. We have then studied the effect of various substitution

DOI: 10.1021/acs.inorgchem.5b00834
Inorg. Chem. 2015, 54, 6547−6559

Table 2. Calculated Bond Angles (deg) and Bond Distances (Å) for Several Model Complexes $[FeX_2(SR_2)\{R^1{}_2PN(R^2)P'R^3{}_2\}]$ in the High-Spin State

R	R^1	R^2	R^3	notes[a]	P−M−P′[b]	P−N−P′	Fe−P	Fe−P′	Fe−S	Δ*d*
H	Ph	Me	Me		69.3	107.7	2.454	2.517	2.750	0.063
Me	Me	Me	Me	*c*	74.4	106.7	2.142	2.221	2.231	0.079
Me	Me	Me	Me	*d*	73.9	98.1	2.155	2.229	2.303	0.074
H	H	Me	Me		69.1	108.5	2.458	2.528	2.739	0.070
H	H	H	Me		69.3	110.9	2.473	2.554	2.729	0.081
Me	Ph	Me	Me		68.7	108.1	2.464	2.557	2.606	0.093
H	Me	Me	Me		70.0	108.1	2.428	2.523	2.748	0.095
H	Me	H	Me		70.0	111.1	2.444	2.559	2.734	0.115
Me	H	Me	Me		68.5	108.9	2.456	2.578	2.599	0.122
Me	Me	Me	Me	min[e]	69.1	108.5	2.432	2.565	2.609	0.133
Me	Me	Me	Me	TS[f]	69.3	107.7	2.481	2.483	2.689	0.002
Me	H	H	Me		68.7	111.5	2.468	2.613	2.592	0.145
Me	Me	H	Me		69.3	111.8	2.446	2.612	2.598	0.166
H	Ph	Me	Ph		68.8	108.9	2.426	2.610	2.773	0.184
H	Me	Me	Ph		68.6	108.5	2.411	2.621	2.777	0.210
H	Me	Me	H		68.4	109.5	2.416	2.635	2.689	0.219
H	H	Me	H		67.6	109.3	2.435	2.656	2.675	0.221
H	H	H	Ph		68.1	111.3	2.446	2.668	2.734	0.222
H	Ph	H	Ph		68.7	112.5	2.442	2.669	2.736	0.227
H	H	H	H		67.7	112.1	2.442	2.707	2.664	0.265
Me	Ph	Me	Ph		67.6	109.9	2.432	2.703	2.609	0.271
		3 (exp)			64.5	111.7	2.457	2.798	2.580	0.341
H	Me	H	H		68.2	112.2	2.422	2.705	2.674	0.283
H	Ph	H	H		67.6	112.0	2.436	2.731	2.662	0.295
Me	Me	Me	Ph		67.3	109.4	2.409	2.725	2.611	0.316
Me	Me	H	H		61.5	118.3	2.393	3.262	2.511	0.869
Me	H	Me	H		57.6	114.6	2.379	3.413	2.493	1.034
Me	H	H	H		57.2	119.2	2.382	3.524	2.489	1.142
Me	Me	Me_2		*g*			2.391		2.485	

[a]X = Cl^- unless otherwise specified. [b]The average P−M−P′ bite angle for bidentate $R^1{}_2PN(R^2)P'R^3{}_2$ ligands in structures found in the CSD is 71(2)°; bite angles reported for DRPM, DRPE, and DRPP ligands[24] are 72(2), 86(3), and 93(4)°, respectively. [c]X = CN^- (low spin). [d]Low spin. [e]Energy minimum. [f]Transition state. [g]Four-coordinate complex $[FeCl_2(SR_2)(R^1_2PNMe_2)]$.

patterns in a series of 24 molecules of general formula $[FeCl_2(SR_2)\{R^1_2PN(R^2)P'R^3_2\}]$ in the high-spin state, where R = H, Me; R^1, R^2, and R^3 = H, Me, Ph, and some relevant geometrical parameters are presented in Table 2. A significant trend in this series of complexes is the presence of a varying degree of unsymmetry in the two Fe−P bonds, calibrated by the difference between the two distances Δ*d* (Figure 4) with values between 0.07 and 0.32 Å for most of them, in excellent agreement with the structural data for **3** and **4** presented in this work, while the three complexes with R = Me and R^3 = H present a much higher unsymmetry.

The correlation between Δ*d* and Fe−P′ indicates that the different substitution patterns at the diphosphinoamine result in an approximately rigid rotation of the P−N−P′ skeleton around the Fe atom that shortens the Fe−P and at the same time elongates the Fe−P′ distance, resulting in varying degrees of unsymmetry in the chelate ring.

By looking at the variations of the Fe−S and Fe−P′ distances when only one of the four substituents is changed, we conclude that substituents at the more strongly bound phosphorus atom (R^1) and at the nitrogen atom (R^2) have a minor effect, while those at sulfur (R) or at the more weakly bound phosphorus atom (R^3) strongly affect those distances. We have therefore grouped the molecules according to the nature of the thioether, SMe_2 or SH_2, and the R^3 substituent at P′ (Figure 5). It can be clearly seen that (a) the stronger donor character of SMe_2

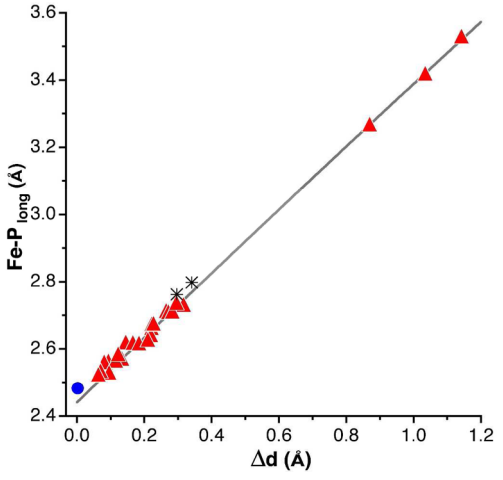

Figure 4. Long Fe−P′ distance in the high-spin complexes $[FeCl_2(SR_2)\{R^1_2PN(R^2)P'R^3_2\}]$ (R = H, Me; R^1, R^2, and R^3 = H, Me, Ph) plotted as a function of the degree of unsymmetry between the two Fe−P bond distances (Δ*d*) in bidentate diphosphinoamines (▲), optimized at the BP86 level, including a transition state for $[FeCl_2(SMe_2)\{Me_2PN(Me)PMe_2\}]$ (●) and the corresponding values in the experimental structures **3** and **4** (∗). Geometric parameters are given in Table 2.

DOI: 10.1021/acs.inorgchem.5b00834
Inorg. Chem. 2015, 54, 6547−6559

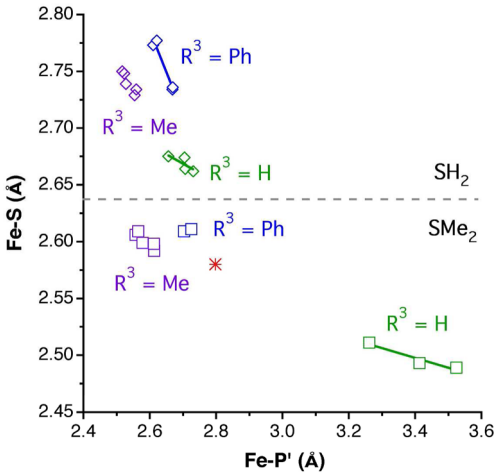

Figure 5. Scatter plot of the long Fe−P′ vs the Fe−S bond distances in the series of calculated complexes $[FeCl_2(SR_2)\{R^1_2PN(R^2)P'R^3_2\}]$ (R = H, Me; R^1, R^2, R^3 = H, Me, Ph). The asterisk indicates the experimental values for **3**.

results in a systematic weakening of the trans Fe−P′ bond and (b) the nature of R^3 affects the strength of the Fe−P′ bond in the order H < Ph < Me, that is, according to the increasing basicity of the phosphine, and conversely for the Fe−S bond. In summary, these results indicate a strong mutual trans influence between the Fe−S and Fe−P′ bonds, whose strengths are modulated by the electron donor properties of the substituents at these atoms. Consistently, the practically nonbonding Fe−P′ distances longer than 3.0 Å (i.e., the most unsymmetrically chelated complexes) correspond to those cases in which a poor donor PH_2 group occupies the position trans to a strong SMe_2 donor ligand.

The varying degree of unsymmetry of the diphosphinoamine chelate ring in the set of model Fe(II) complexes studied suggests a rather flat potential energy surface for the exchange of the strongly and weakly coordinated P atoms passing through a symmetric transition state (Figure 6). We were able

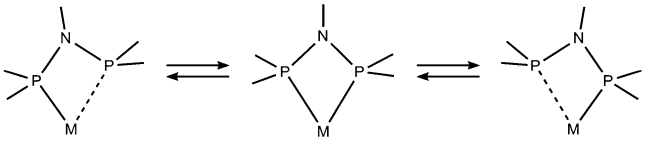

Figure 6. Interconversion between two unsymmetrically coordinated phosphorus atoms of DPPA-type ligands.

to characterize the transition state for the permethylated complex ($R^1 = R^2 = R^3$ = Me), which appears at the symmetric end ($\Delta d \approx 0$) of Figure 4, well-aligned with the general trend shown by the calculated energy minima. The transition state structure deviates from trigonal bipyramidal only because of the small bite angle of the chelating ligand (P−Fe−P = 69°), and the free energy barrier for such a process is estimated at $\Delta G‡$ = 3.2 kcal/mol.

We observe that the less sterically congested complexes containing symmetrically substituted bidentate ligands $[FeCl_2(SH_2)(H_2PNHPH_2)]$ and $[FeCl_2(SMe_2)\{Me_2PN(Me)PMe_2\}]$ show a significant unsymmetric coordination, thus ruling out steric congestion as the main reason for that unsymmetry. This conclusion is supported by the structural characterization of complex **6**, a cationic iron(II) complex bis-chelated by two ligands **2** and further chelated by an acetate ligand (see previous section). Despite a more sterically congested coordination sphere and thus anticipated enhanced steric repulsion, no uncommon Fe−P bond length was observed. All these observations indicate that the reasons behind such a binding unsymmetry are electronic in origin. The most common symmetric coordination mode found in other complexes of the same bidentate ligand appears here only as a transition state between two unsymmetric forms.[5,8a,10]

Having analyzed the electronic and steric effects of the substituents on the unsymmetry of the chelate ring in our calculated high-spin Fe(II) complexes, we must now compare these results with experimental and calculated data for low-spin species. Our calculations for the low-spin excited state of the permethylated complex (R = R^1 = R^2 = R^3 = Me, third entry in Table 2) and for the low-spin ground state of the analogous complex with cyanido ligands replacing the chlorido ligands (second entry in Table 2) afford much shorter Fe−P bond distances and a rather small unsymmetry of the chelate (with $\Delta d \leq 0.08$ Å), features that appear also in complex **6**. Although we have found no precedent of five-coordinate Fe(II) complexes with PNP ligands, all six-coordinate Fe(II) complexes, five-coordinate compounds with iron in other oxidation states, and complexes with other metals in a low-spin state present similar bonding characteristics, as seen in Figure 7 (data provided in the Supporting Information, Table S2).

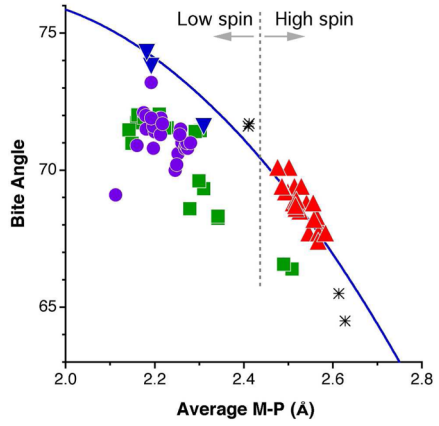

Figure 7. Scatter plot of the calculated average Fe−P bond distances and bite angles in the series of high- (▲) and low-spin (▼) Fe(II) complexes with SR_2 and $R^1_2PN(R^2)PR^3_2$ ligands (Table 2). Experimental data for related complexes of iron (●) and other metals (■) also shown for comparison. Compounds **3**−**6** are represented by asterisks, and the continuous line corresponds to a least-squares fitting of the calculated values (three points with M−P > 2.8 Å not shown were included in the fitting).

In Figure 7 we can see a clear dividing line between the low-spin and high-spin complexes, regardless of the metal atom, its oxidation state, and its coordination number. Remarkably, the two PNP chelate rings in a high-spin Cr(II) compound[26] appear in the same region as the Fe(II) high-spin complexes. A smaller bite angle associated with longer metal−ligand distances in the high-spin state is a well-known consequence of the approximately rigid bite of bidentate ligands.[27,28] However, we find that in this family, the ligands seem to be more flexible than expected, since the P−Fe−P′ bite angles vary between 64 and 74° in all compounds analyzed (independently of the spin state and similarly in calculated and experimental structures),

DOI: 10.1021/acs.inorgchem.5b00834
Inorg. Chem. 2015, 54, 6547−6559

whereas the P−N−P′ bond angle varies twice as much, between 92 and 112° (92−103° for low-spin, 107−112° for high-spin complexes, comprising both experimental and calculated values), as schematically shown in Figure 8. We

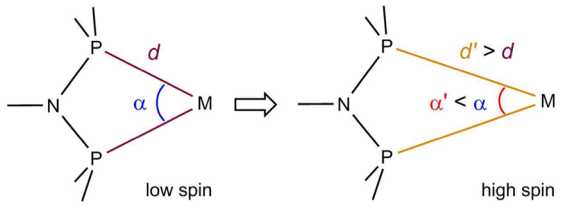

Figure 8. Geometrical differences in the chelate ring formed by PNP ligands between the low- and high-spin states of transition metal complexes: a high average M−P distance is associated with a smaller P−M−P angle and a larger P−N−P angle (see also Figure 7).

note that the bite angles found, which are similar to those in the topologically equivalent diphosphine DPPM complexes, 72(2)°,[28] are rather small compared to the ideal P−M−P bond angle for an equatorial−axial coordination mode in a trigonal bipyramid (90°) and for a basal−basal coordination mode in a square pyramid (86°). Also the P−N−P bond angles are smaller than found for the free ligands (we calculate 121.9° for DPPA, and six PNP uncoordinated ligands found in the CSD, with the same conformation as when chelated, present angles in the range of 111−125°), especially in the low-spin compounds.

We therefore hypothesize that there might be a mismatch between the orientation of the phosphorus lone pair orbitals and the metal acceptor orbitals. To estimate the orientation of the lone pairs at the P atoms in the bidentate ligand, we performed a geometry optimization for a monoprotonated version of DPPA, which forms H−P−N and P−N−P bond angles of 101.0 and 122.5°, respectively. From those values we estimate the ideal bite angle for a chelate ring at 35.5°, much smaller even than the smallest of the experimental bite angles. Since the lone pair orbitals interact with two different orbitals of the d-block set, conveniently hybridized with s and p orbitals (Figure 9), the unsymmetric pseudochelate coordination mode found allows for an improved overlap with one of the acceptor

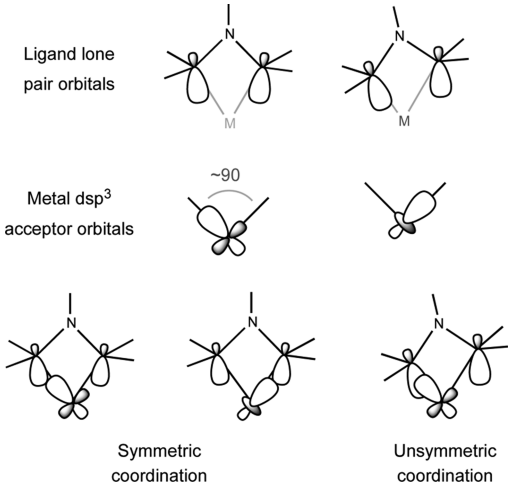

Figure 9. Orientation of the lone pair orbitals of DPPA-type ligands (upper), of the metal dsp^3 hybrids (center), and misalignment of the two types of orbitals (lower).

orbitals at the cost of losing some of the initially poor overlap with the other acceptor orbital, as schematically shown in Figure 9.

To verify the validity of such an explanation, we optimized the geometries of similar molecules having bidentate diphosphines with larger bite angles that fit better with the ideal coordination polyhedra, that is, DPPE and bis(diphenylphosphino)propane (DPPP), whose bite angles are 86(3)° and 93(4)°, respectively.[28] The results, shown in Table 3 and represented along with the related diphosphinoamine complexes in Figure 10, indicate clearly a much smaller degree of Fe−P bonding unsymmetry in the case of the larger bite ligands.

Our results show that analogous bidentate ligands with a larger bite result in stronger binding of the second phosphorus atom (i.e., a more symmetric chelating mode) and the resulting weakening of the trans Fe−S bond. This trend goes to the extreme that for DPPE and DPPP (n = 2, 3; $R^1 = R^3$ = Ph), the optimized structure results in dissociation of the trans ligand, leaving four-coordinate complexes in which the diphosphines are symmetrically coordinated. Note, though, that a non-negligible degree of unsymmetry persists with these ligands, suggesting that the strong donor sulfur atom in trans position is also responsible in part for a weaker Fe−P′ bond.

If a too-small bite angle produces an orbital mismatch between the bidentate ligand and the metal atom, it is now clear that this effect is more pronounced in the high-spin than in the low-spin complexes (Figure 7). The latter present in all cases much smaller degrees of unsymmetry ($\Delta d \leq 0.08$ Å) than the high-spin ones ($0.07 \leq \Delta d \leq 1.14$ Å), with the only exception of a Ru complex,[29] in the region of short M−P distances and slightly overlapping with the region of the calculated values for the high-spin Fe complexes, probably due to steric encumbrance of their two DPPA ligands.

Magnetic Properties. The magnetic behavior of complexes **3** and **4** was in agreement with the conclusions from the theoretical calculations and showed unambiguously quintet ground states for both complexes with no orbital moment contribution, with Curie−Weiss behavior above 50 and 100 K, respectively (Figures S3 and S4 in Supporting Information). For complex **3**, the Curie constant of 3.080(2) cm^3·K·mol^{-1} supports a complex close to an S = 2 distorted tetrahedron with g = 2.026. This is also supported by the presence of temperature-independent paramagnetism as expected for a tetrahedral geometry, where for d^6 Fe(II) a low-lying $^5T_2(^5D)$ excited state with angular momentum is mixed with the ^5E ground state.[30] At lower temperatures, the $\chi_M T$ product increases below 50 K to 3.29 cm^3·K·mol^{-1}, then decreases to 2.02 cm^3·K·mol^{-1} at 1.8 K, showing the occurrence of some ferromagnetic interactions (Figure 11). The isothermal magnetization at 8 K is close to the S = 2 Brillouin curve with g = 2.026 but shows a nesting behavior at lower temperatures that usually points toward magnetic anisotropy (Figure S5 in Supporting Information). The alternating current (ac) susceptibility below 20 K did not show any out-of-phase signal evidencing slow relaxation of the magnetization. All these data point toward isolated Fe(II) magnetic centers, in agreement with the long Fe···Fe distances observed in the crystal structures. We could indeed simulate all the magnetic data considering axial zero-field splitting for the quintet ground state with some ferromagnetic intermolecular interaction introduced with a mean-field correction. Parameters were not unique, but the

DOI: 10.1021/acs.inorgchem.5b00834
Inorg. Chem. 2015, 54, 6547−6559

Table 3. Calculated Bite Angles (deg) and Bond Distances (Å) for Model Complexes with Diphosphines Forming Five- and Six-Membered Chelate Rings, of Formulae $[FeCl_2(SMe_2)\{R^1{}_2P(CH_2)_nP'R^3_2\}]$, Compared with Values for Analogous DPPA-Type Ligands in $[FeCl_2(SMe_2)\{R^1_2PN(H)P'R^3_2\}]$ (with R^1, R^3 = H, Me) Given in Parentheses

R^1, R^3	n	P−M−P′	Fe−P		Fe−P′		Fe−S	
H	2	82.7	2.428	(2.38)	2.539	(3.52)	2.603	(2.49)
	3	88.7	2.417		2.501		2.633	
Me	2	84.4	2.420	(2.45)	2.501	(2.61)	2.647	(2.60)
	3	92.6	2.406		2.478		2.686	

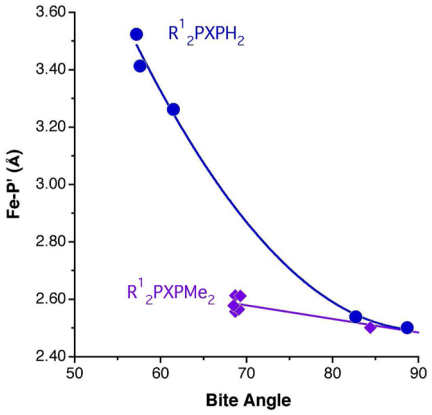

Figure 10. Dependence of the calculated long Fe−P′ bond distance on the bite angle in the series of complexes $[FeCl_2(SMe_2)(R^1{}_2PXPH_2)]$ (●) and $[FeCl_2(SMe_2)(R^1{}_2PXPMe_2)]$ (◆), with X = NMe, C_2H_4, C_3H_6; R^1 = H, Me, Ph.

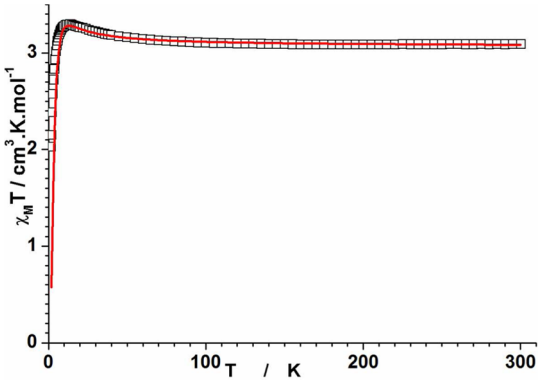

Figure 11. Evolution of the magnetic susceptibility χ_M product with temperature for complex **3**, measured in a static 1 T field, the red line is the fit resulting from the parameters described in the text.

following set was found to be satisfying and reasonable: $g_{\parallel}$ = 2.33, $g_{\perp}$ = 1.85, D = −1.04 cm^{-1}, zJ = +0.04 cm^{-1}.

For complex **4**, the Curie constant of 6.44(1) cm^3·K·mol^{-1} evidences a quintet ground state for both Fe(II) centers. The Weiss temperature θ = +11.6(2) K supports the presence of ferromagnetic interactions clearly stronger than for complex **3** (for which θ = −0.4(1) K), something that could be expected given the chlorido bridges. Accordingly, at lower temperatures the $\chi_M T$ product increases strongly below 100 K, to 21.5 cm^3·K·mol^{-1} at 3 K, and then decreases slightly to 20.6 cm^3·K·mol^{-1} at 1.8 K (Figure 12). These values are higher than the 10.0 cm^3·K·mol^{-1} expected for an S = 4 ground state, which would result from an intradimer ferromagnetic coupling. No out-of-phase component of the *ac* susceptibility could be evidenced between 2 and 15 K. The isothermal magnetization curves between 8 and 1.8 K are almost superimposed, above the Brillouin curves

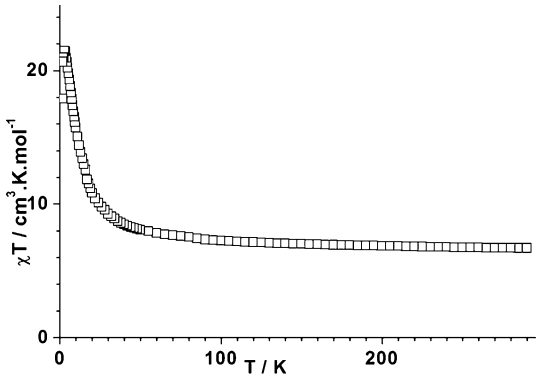

Figure 12. Evolution of the magnetic susceptibility χ_M product with temperature for complex **4**, measured in a static 0.1 T field.

for both S = 2 and S = 4 ground states with g = 2.18 (Figure 13), but very close to the curve obtained by considering a third

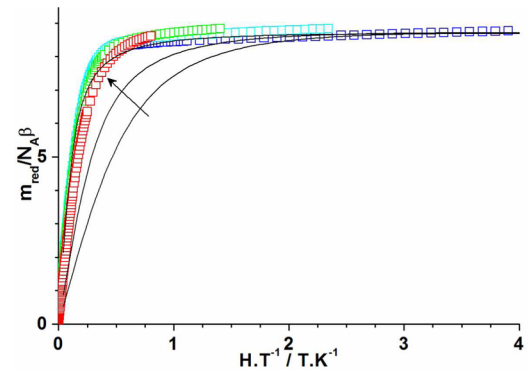

Figure 13. Plots of the reduced isothermal magnetization vs field for complex **4** (1.8 (dark blue), 3 (light blue), 5 (green) and 8 (red) K). Black lines are the Brillouin curves corresponding successively to two S = 2 with g = 2.18, one S = 4 with g = 2.18, and 1/3× one S = 12 with g = 2.17.

of the Brillouin curve for an S = 12 ground state with g = 2.17. This would point toward ferromagnetic intermolecular interactions with two neighboring complexes, but no evidence of this could be found in the 173 K X-ray structure. A possible explanation could be a crystallographic phase transition at lower temperatures with a tripling of the unit cell, where those interactions could take place. The low $\chi_M T$ value measured at 3 K respective to the 78.0 cm^3·K·mol^{-1} expected for an S = 12 ground state can then be easily accounted for by dipolar antiferromagnetic interactions between those entities. Nevertheless, in the absence of a clear structural model, we did not try further to simulate the magnetic data.

DOI: 10.1021/acs.inorgchem.5b00834
Inorg. Chem. 2015, 54, 6547−6559

CONCLUSION

In this work, we provided novel examples showing how subtle changes in a ligand can result in the formation of complexes with very different structures and magnetic properties. Thus, despite the close similarity between the two short-bite ligands $(Ph_2P)_2N(CH_2)_3SMe$ (**1**) and $(Ph_2P)_2N(p\text{-}C_6H_4)SMe$ (**2**), their Fe(II) complexes $[FeCl_2(\mathbf{1})]_n$ (**3**) and $[FeCl_2(\mathbf{2})]_2$ (**4**) adopt a very different structure in the solid state, although they were obtained under strictly similar synthetic and crystallization conditions. Whereas **3** is a coordination polymer in which ligand **1** acts as a *P*,*P*-pseudochelate and a (*P*,*P*),*S*-bridge, **4** is a chlorido-bridged dimer in which ligand **2** acts only as a *P*,*P*-pseudochelate. This difference was found to be due to the different nature of the spacer between the nitrogen atom and the −SMe group, which is flexible in **3** but rigid in **4**. The examination of the solid-state structures ruled out an explanation based on packing effects. It was intriguing to find that in both complexes, one Fe−P bond length is unusually long, leading to an unsymmetrical behavior of the potentially chelating short-bite diphosphine ligand. The results of a theoretical analysis and of the synthesis and structural analysis of the sterically more congested complex $[Fe(OAc)(\mathbf{2})_2]PF_6$ (**6**) concluded for the involvement of electronic rather than steric factors to explain these unusual features. Our DFT calculations on high-spin iron(II) complexes of general formula $[FeCl_2(SR_2)\{R^1_2PN(R^2)PR^3_2\}]$ (R = H, Me; R^1, R^2, and R^3 = H, Me, Ph) reveal the existence of a varying degree of unsymmetry for the two Fe−P bonds, calibrated by values in the range of 0.07−0.32 Å for the distance difference Δd. A correlation between Δd and the longest Fe−P′ distance indicates a rigid rotation of the PNP ligand skeleton around the Fe atoms from a nearly symmetric to a strongly unsymmetric coordination. The exchange between the positions of the two P atoms can proceed through a symmetrically coordinated transition state, with a calculated free energy of activation of 3.2 kcal/mol. An analysis of a variety of substitution patterns of the thioether and diphosphinoamine ligands shows that substituents at the more strongly bound phosphorus atom and at the N atom have a minor effect on the Fe−S and Fe−P bond distances, whereas substituents at the weakly bound P or at the sulfur atom strongly affect those two distances. Thus, the stronger basic character of SMe_2, compared to SH_2, results in a systematic weakening of the trans Fe−P′ bond, and the nature of the substituents at the weakly bound phosphorus favors stronger Fe−P′ bonds in the order of Me > Ph > H, indicating a strong mutual trans influence of the Fe−S and Fe−P′ bonds, which makes one of them weaker as the other becomes stronger and vice versa. The influence of the substituents at those two donor atoms is associated with the inductive effects that modulate their basicity, while steric effects can be ruled out within the wide family of computational models used.

The low-spin model complex $[Fe(CN)_2(SMe_2)(Me_2PN(Me)PMe_2)]$ and the excited low-spin state of $[FeCl_2(SMe_2)(Me_2PN(Me)PMe_2)]$ present shorter Fe−P distances and a much more symmetric chelation of the PNP ligand than found for the high-spin complexes studied. A structural analysis of complexes with PNP ligands shows that our conclusions can be made more general: the low-spin complexes with these ligands have shorter Fe−P distances and more symmetric chelation than the high-spin ones, regardless of the nature of the metal, its oxidation state, and its coordination number.

The nonsymmetric bonding mode of the PN(R)P ligands has been found to be due not only to a combination of mismatch between the orientation of the phosphorus lone pair orbitals and the metal acceptor orbitals but also to the strong trans influence of the thioether ligand. The orbital mismatch must be attributed to their very small bite angles, since related ligands with larger bite angles are seen to present a much smaller degree of chelate unsymmetry. A further consequence of the more symmetric chelate rings with shorter Fe−P′ bond distances is a weakening of the trans Fe−S bond.

Magnetic measurements on complexes **3** and **4** confirmed an $S = 2$ ground state, evidencing that, from the magnetic point of view, the coordination geometry of these complexes may be considered as distorted tetrahedral. While only weak intermolecular ferromagnetic interactions could be evidenced for complex **3**, stronger ferromagnetic interactions, both intra- and intermolecular, were evidenced for complex **4**, though it is likely that a modification of the crystal packing occurs at low temperatures.

In view of the versatility of the coordination chemistry observed in this work with the functional short-bite ligands **1** and **2**, further work is in progress to extend the study of their behavior to other transition metals able to display variable coordination spheres.

EXPERIMENTAL SECTION

All manipulations were performed by using standard Schlenk techniques under an inert atmosphere. Solvents were purified and dried under a nitrogen atmosphere by using conventional methods. FT-IR spectra were recorded in the region of 4000−650 cm^{-1} on a Nicolet 380 FTIR spectrometer (ATR mode, ZnSe crystal). Elemental analyses were performed by the "Service de Microanalyses", Université de Strasbourg. ESI-MS spectra were recorded on a microTOF (Bruker Daltonics, Bremen, Germany) instrument, using nitrogen as drying agent and nebulizing gas. The ligands bis(diphenylphosphino)(*N*-(methylthio)propyl)amine $(Ph_2P)_2N(CH_2)_3SMe$ (**1**)[7f] and bis(diphenylphosphino)(*N*-4-(methylthio)phenyl)amine $(Ph_2P)_2N(p\text{-}C_6H_4)SMe$ (**2**)[8a] were prepared according to literature procedures. All other reagents were used as received from commercial suppliers. Magnetic data were recorded using a MPMS-7XL Quantum Design SQUID magnetometer. Magnetic susceptibilies were measured using an RSO probe between 1.8 and 300 K under 1 and 10 kOe applied field, on polycrystalline samples enclosed in heat-sealed 30 μm thick polyethylene bags accurately weighed with a Mettler MX5 microbalance. Magnetizations were measured at 1.8, 3, 5, and 8 K in the 0−70 kOe range, and *ac* susceptibility data were measured at 100 and 1000 Hz with a 3 Oe amplitude. Data were corrected using multipole expansion, and sample holder contribution was accounted for by a combination of a diamagnetic and a Curie tail for the polyethylene bag.[31] The samples diamagnetic contributions were approximated with -300×10^{-6} $cm^3 \cdot mol^{-1}$ (**3**) and -635×10^{-6} $cm^3 \cdot mol^{-1}$ (**4**), respectively. A temperature-independent paramagnetic contribution of $+250 \times 10^{-6}$ $cm^3 \cdot mol^{-1}$ was also considered for complex **3**. Magnetic data were fitted using the program PHI.[32]

Complex 3, $[FeCl_2(1)]_n$. To a suspension of anhydrous $FeCl_2$ (0.127 g, 1.06 mmol) in CH_2Cl_2 (10 mL) was added a solution of ligand **1** (0.500 g, 1.06 mmol) in CH_2Cl_2 (20 mL). The color of the solution quickly turned to pink, and stirring was maintained at room temperature for 12 h. The solution was concentrated to a third of its original volume, and crystallization by slow diffusion of pentane afforded yellow crystals of complex **3**. Yield: 0.545 g (86%). Anal. Calcd for $C_{28}H_{29}Cl_2FeNP_2S$ (600.30): C, 56.02; H, 4.87; N, 2.33. Found: C, 55.71; H, 4.66; N, 2.57%. FTIR: ν_{max}(solid)/cm^{-1}: 3053vw, 2915vw, 2866vw, 1481w, 1432m, 1186w, 1159vw, 1090s, 1068m, 1028w, 997w, 960w, 880vs, 789s, 746s, 739s. MS (ESI): *m*/*z* (ranked by decreasing intensity) = 1037.2 $[FeCl(\mathbf{1})_2]^+$, 474.2 $[\mathbf{1}+H]^+$, 501.1

DOI: 10.1021/acs.inorgchem.5b00834
Inorg. Chem. 2015, 54, 6547−6559

$[Fe(\mathbf{1})]^{2+}$. Yellow crystals suitable for single-crystal X-ray diffraction were grown from a mixture of CH_2Cl_2/pentane.

Complex 4, $[FeCl_2(2)]_2$. The same procedure was used with anhydrous $FeCl_2$ (0.075 g, 0.59 mmol) and ligand **2** (0.300 g, 0.59 mmol), affording orange crystals of complex **4**. Yield: 0.320 g (85%). Anal. Calcd for $C_{62}H_{54}Cl_4Fe_2N_2P_4S_2$ (1268.63): C, 58.70; H, 4.29; N, 2.21. Found: C, 58.36; H, 4.04; N, 1.97%. FTIR: ν_{max}(solid)/cm^{-1}: 1589w, 1492m, 1480w, 1434m, 1310w, 1255s, 1182w, 1162s, 1096s, 1071w, 997w, 952s, 907vs, 855w, 823m, 749s, 737s. MS (ESI): m/z (ranked by decreasing intensity) = 598.0 $[FeCl(\mathbf{2})]^+$ or $[M\text{-}2Cl]^{2+}$, 1071.2 $[Fe(\mathbf{2})_2+H]^+$, 1105.2 $[FeCl(\mathbf{2})_2]^+$, 1233.0 $[M\text{-}Cl]^+$, 1291.6 $[M+Na]^+$. Orange crystals suitable for single-crystal X-ray diffraction were grown from a mixture of CH_2Cl_2/pentane.

Complex 5, $[Fe(OAc)(1)_2]PF_6$. In a glovebox, dry CH_2Cl_2 (10 mL) was added at room temperature to solid anhydrous $[Fe(OAc)_2]$ (0.037 g, 0.21 mmol), ligand **1** (0.200 g, 0.42 mmol), and anhydrous $LiPF_6$ (0.128 g, 0.84 mmol), and the resulting yellowish suspension was stirred overnight at room temperature. The mixture turned to pink-red, and the suspension was filtered through a pad of diatomaceous earth, and the volatiles were removed under vacuum. The resulting red sticky solid was washed twice with pentane and dried, affording complex **5** as a red solid. Yield: 0.158 g (62%). Anal. Calcd for $C_{58}H_{61}F_6FeN_2O_2P_5S_2$ (1206.96): C, 57.72; H, 5.09; N, 2.32. Found: C, 57.69; H, 5.11; N, 2.35%. FTIR: ν_{max}(solid)/cm^{-1}: 3052w, 2915w, 2854w, 1964vw, 1891vw, 1824vw, 1585w, 1479m (OAc), 1434s (OAc), 1308m, 1182m, 1106sh, 1090s, 1065s, 1026m, 998m, 955w, 918w, 835vs (PF_6), 740vs MS (ESI): m/z = 1061.25 $[M\text{-}PF_6]^+$.

Complex 6, $[Fe(OAc)(2)_2]PF_6$. The same procedure was used with anhydrous $[Fe(OAc)_2]$ (0.034 g, 0.20 mmol), ligand **2** (0.200 g, 0.39 mmol), and anhydrous $LiPF_6$ (0.120 g, 0.79 mmol), affording complex **6** as a red solid. Yield: 0.184 g (73%). Anal. Calcd for $C_{64}H_{57}F_6FeN_2O_2P_5S_2$ (1275.00): C, 60.29; H, 4.51; N, 2.20. Found: C, 60.36; H, 4.55; N, 2.14%. FTIR: ν_{max}(solid)/cm^{-1}: 3052w, 2918w, 1958vw, 1892vw, 1815vw, 1595m, 1585sh, 1498s (OAc), 1479sh, 1433s (OAc), 1397w, 1368w, 1292m, 1268m, 1182m, 1093s, 1069s, 1026m, 1013m, 998m, 968w, 951w, 924w, 883sh, 838vs (PF_6), 740vs MS (ESI): m/z = 1129.21 $[M\text{-}PF_6]^+$. Red crystals suitable for single-crystal X-ray diffraction were grown from a mixture of CH_2Cl_2/pentane.

Crystal Structure Determinations. Crystals of **3**, **4**, and **6** were obtained as described above. The crystals were placed in oil, and a single crystal was selected, mounted on a glass fiber and placed in a low-temperature N_2 stream. X-ray diffraction data collection was performed at 173(2) K on a Nonius Kappa-CCD diffractometer[33] equipped with an Oxford Cryosystem liquid N_2 device, using graphite-monochromated Mo Kα radiation (λ = 0.710 73 Å). The crystal-detector distance was 36 mm. Crystallographic and experimental details for the structures are summarized in Table S1 in the Supporting Information. The structures of **3**, **4**, and **6** were solved by direct methods using the program SHELXS-97.[34] The refinement and all further calculations were performed using SHELXL-97[35] or SHELX-2013.[36] The H atoms were included in calculated positions and treated as riding atoms using SHELXL default parameters.

Computational Details. All calculations were performed with the Gaussian09 code[37] at the generalized gradient DFT level, using the BP86 method that adopts the Becke exchange[38] and Perdew correlation[39] functionals. This nonhybrid functional solved the problems found with other functionals in the description of the calculated bond distances and the unsymmetry (described as the difference between the two Fe−P distances Δd), giving highly consistent results compared to the experimental structures (see Supporting Information). It must be said that a host of calculations with the B3LYP and B97D functionals gave results qualitatively consistent with the BP86 ones reported here. The all electron triple-ζ basis set proposed by Schäfer et al.[40] was used for all the atoms. All the energy minima and a transition state were characterized by vibrational analyses.

■ ASSOCIATED CONTENT

Ⓢ Supporting Information

X-ray data collection and structure refinement for all compounds. CCDC numbers 1014960−1014962 (**3**, **4**, and **6**). Histograms representing the distribution of the Fe−P distances in the structures available in the CCDC. Bite angles, M−P distances, and M−P distance unsymmetry (Δd) in structures of PNP complexes, atomic coordinates of the optimized model complexes and ligands, and Curie−Weiss and isothermal reduced magnetization plots for complexes **3** and **4**. The Supporting Information is available free of charge on the ACS Publications website at DOI: 10.1021/acs.inorgchem.5b00834.

■ AUTHOR INFORMATION

Corresponding Authors

*E-mail: santiago.alvarez@qi.ub.es. (S.A.)

*E-mail: braunstein@unistra.fr. (P.B.)

Present Address

▽REQUIMTE, Departamento de Química, Faculdade de Ciências e Tecnologia, Universidade Nova de Lisboa, Caparica, 2829−516, Portugal.

Notes

The authors declare no competing financial interest.

■ ACKNOWLEDGMENTS

We are grateful to the CNRS, the Ministère de la Recherche (Paris), the DFH/UFA (International Research Training Group 532-GRK532, Ph.D. grant to C.F.), the Spanish Ministerio de Economía y Competitividad (Project No. CTQ2011-23862-C02-01) and the Fundação para a Ciência e Tecnologia (FCT; fellowships SFRH/BPD/73253/2010 to C.F. and SFRH/BPD/44262/2008 to V.R.) for funding. We thank the "Service de radiocrystallographie" from the Université de Strasbourg (France) and Dr. R. Pattacini for performing the X-ray diffraction studies and Dr. D. Specklin for the graphical Figures 1−3.

■ REFERENCES

(1) Selected reviews: (a) Appleby, T.; Woollins, J. D. *Coord. Chem. Rev.* **2002**, *235*, 121−140. (b) Bhattacharyya, P.; Woollins, J. D. *Polyhedron* **1995**, *14*, 3367−3388. (c) Haiduc, I.; Silaghi-Dumitrescu, I. *Coord. Chem. Rev.* **1986**, *74*, 127−270.

(2) Selected recent examples of metal complexes of N-functionalized DPPA-type ligands applied to catalytic processes (more are given in refs 6−9:): (a) Ok, F.; Aydemir, M.; Durap, F. *Appl. Organomet. Chem.* **2014**, *28*, 38−43. (b) Aydemir, M.; Meric, N.; Kayan, C.; Ok, F.; Baysal, A. *Inorg. Chim. Acta* **2013**, *398*, 1−10. (c) Cheung, H. W.; So, C. M.; Pun, K. H.; Zhou, Z.; Lau, C. P. *Adv. Synth. Catal.* **2011**, *353*, 411−425. (d) Aydemir, M.; Baysal, A.; Özkar, S.; Yıldırım, L. T. *Inorg. Chim. Acta* **2011**, *367*, 166−172. (e) Aydemir, M.; Baysal, A.; Özkar, S.; Yıldırım, L. T. *Polyhedron* **2011**, *30*, 796−804.

(3) (a) Rosa, V.; Fliedel, C.; Ghisolfi, A.; Pattacini, R.; Avilés, T.; Braunstein, P. *Dalton Trans.* **2013**, *42*, 12109−12119. (b) Ghisolfi, A.; Fliedel, C.; Rosa, V.; Pattacini, R.; Thibon, A.; Yu. Monakhov, K.; Braunstein, P. *Chem.—Asian J.* **2013**, *8*, 1795−1805. (c) Fliedel, C.; Pattacini, R.; Braunstein, P. *J. Cluster Sci.* **2010**, *21*, 397−415. (d) Rodriguez-Zubiri, M.; Gallo, V.; Rosé, J.; Welter, R.; Braunstein, P. *Chem. Commun.* **2008**, 64−66. (e) Gallo, V.; Mastrorilli, P.; Nobile, C. F.; Braunstein, P.; Englert, U. *Dalton Trans.* **2006**, 2342−2349. (f) Choualeb, A.; Braunstein, P.; Rosé, J.; Bouaoud, S.-E.; Welter, R. *Organometallics* **2003**, *22*, 4405−4417. (g) Bachert, I.; Braunstein, P.; McCart, M. K.; Fabrizi de Biani, F.; Laschi, F.; Zanello, P.; Kickelbick, G.; Schubert, U. *J. Organomet. Chem.* **1999**, *573*, 47−59. (h) Bachert,

DOI: 10.1021/acs.inorgchem.5b00834
Inorg. Chem. 2015, 54, 6547−6559

I.; Braunstein, P.; Guillon, E.; Massera, C.; Rosé, J.; DeCian, A.; Fischer, J. *J. Cluster Sci.* **1999**, *10*, 445−458. (i) Bachert, I.; Bartusseck, I.; Braunstein, P.; Guillon, E.; Rosé, J.; Kickelbick, G. *J. Organomet. Chem.* **1999**, *580*, 257−264. (j) Bachert, I.; Braunstein, P.; Hasselbring, R. *New J. Chem.* **1996**, *20*, 993−995.

(4) (a) Schweyer-Tihay, F.; Braunstein, P.; Estournès, C.; Guille, J. L.; Lebeau, B.; Paillaud, J. L.; Richard-Plouet, M.; Rosé, J. *Chem. Mater.* **2002**, *15*, 57−62. (b) Braunstein, P.; Kormann, H.-P.; Meyer-Zaika, W.; Pugin, R.; Schmid, G. *Chem.—Eur. J.* **2000**, *6*, 4637−4646. (c) Lin, B.; Liu, Z.; Liu, M.; Pan, C.; Ding, J.; Wu, H.; Cheng, J. *Catal. Commun.* **2007**, *8*, 2150−2152.

(5) Fliedel, C.; Faramarzi, V.; Rosa, V.; Doudin, B.; Braunstein, P. *Chem.—Eur. J.* **2014**, *20*, 1263−1266.

(6) For general and recent reviews, see, for example: (a) Dagorne, S.; Fliedel, C. *Top. Organomet. Chem.* **2013**, *41*, 125−171. (b) McGuinness, D. S. *Chem. Rev.* **2011**, *111*, 2321−2341. (c) Agapie, T. *Coord. Chem. Rev.* **2011**, *255*, 861−880. (d) van Leeuwen, P. W. N. M.; Clément, N. D.; Tschan, M. J. L. *Coord. Chem. Rev.* **2011**, *255*, 1499−1517. (e) Dixon, J. T.; Green, M. J.; Hess, F. M.; Morgan, D. H. *J. Organomet. Chem.* **2004**, *689*, 3641−3668.

(7) For recent research articles, see, for example: (a) Britovsek, G. J. P.; McGuiness, D. S.; Wierenga, T. S.; Young, C. T. *ACS Catal.* **2015**, *5*, 4152−4166. (b) Suttil, J. A.; Wasserscheid, P.; McGuinness, D. S.; Gardiner, M. G.; Evans, S. J. *Catal. Sci. Technol.* **2014**, *4*, 2574−2588. (c) Sa, S.; Lee, S. M.; Kim, S. Y. *J. Mol. Catal. A: Chem.* **2013**, *378*, 17−21. (d) Liu, S.; Pattacini, R.; Braunstein, P. *Organometallics* **2011**, *30*, 3549−3558. (e) Aluri, B. R.; Peulecke, N.; Peitz, S.; Spannenberg, A.; Müller, B. H.; Schulz, S.; Drexler, H.-J.; Heller, D.; Al-Hazmi, M. H.; Mosa, F. M.; Wöhl, A.; Müller, W.; Rosenthal, U. *Dalton Trans.* **2010**, *39*, 7911−7920. (f) Weng, Z.; Teo, S.; Hor, T. S. A. *Dalton Trans.* **2007**, 3493−3498. (g) Killian, E.; Blann, K.; Bollmann, A.; Dixon, J. T.; Kuhlmann, S.; Maumela, M. C.; Maumela, H.; Morgan, D. H.; Nongodlwana, P.; Overett, M. J.; Pretorius, M.; Höfener, K.; Wasserscheid, P. *J. Mol. Catal. A: Chem.* **2007**, *270*, 214−218. (h) Blann, K.; Bollmann, A.; de Bod, H.; Dixon, J. T.; Killian, E.; Nongodlwana, P.; Maumela, M. C.; Maumela, H.; McConnell, A. E.; Morgan, D. H.; Overett, M. J.; Prétorius, M.; Kuhlmann, S.; Wasserscheid, P. *J. Catal.* **2007**, *249*, 244−249.

(8) Selected recent examples: (a) Ghisolfi, A.; Fliedel, C.; Rosa, V.; Yu. Monakhov, K.; Braunstein, P. *Organometallics* **2014**, *33*, 2523−2534. (b) Boulens, P.; Lutz, M.; Jeanneau, E.; Olivier-Bourbigou, H.; Reek, J. N. H.; Breuil, P.-A. R. *Eur. J. Inorg. Chem.* **2014**, 3754−3762. (c) Song, K.; Gao, H.; Liu, F.; Pan, J.; Guo, L.; Zai, S.; Wu, Q. *Eur. J. Inorg. Chem.* **2009**, 3016−3024.

(9) Selected recent examples: (a) Kayan, C.; Biricik, N.; Aydemir, M.; Scopelliti, R. *Inorg. Chim. Acta* **2012**, *385*, 164−169. (b) Kayan, C.; Biricik, N.; Aydemir, M. *Transition Met. Chem.* **2011**, *36*, 513−520. (c) Aydemir, M.; Baysal, A.; Sahin, E.; Gumgum, B.; Ozkar, S. *Inorg. Chim. Acta* **2011**, *378*, 10−18. (d) Biricik, N.; Kayan, C.; Gümgüm, B.; Fei, Z.; Scopelliti, R.; Dyson, P. J.; Gürbüz, N.; Özdemir, İ. *Inorg. Chim. Acta* **2010**, *363*, 1039−1047. (e) Akba, O.; Durap, F.; Aydemir, M.; Baysal, A.; Gümgüm, B.; Özkar, S. *J. Organomet. Chem.* **2009**, *694*, 731−736. (f) Biricik, N.; Durap, F.; Kayan, C.; Gümgüm, B.; Gürbüz, N.; Özdemir, İ.; Ang, W. H.; Fei, Z.; Scopelliti, R. *J. Organomet. Chem.* **2008**, *693*, 2693−2699. (g) Aydemir, M.; Baysal, A.; Gümgüm, B. *J. Organomet. Chem.* **2008**, *693*, 3810−3814. (h) Zhang, J.; Braunstein, P.; Hor, T. S. A. *Organometallics* **2008**, *27*, 4277−4279. (i) Gümgüm, B.; Biricik, N.; Durap, F.; Özdemir, I.; Gürbüz, N.; Ang, W. H.; Dyson, P. J. *Appl. Organometal. Chem.* **2007**, *21*, 711−715.

(10) Ghisolfi, A.; Condello, F.; Fliedel, C.; Rosa, V.; Braunstein, P. *Organometallics* **2015**, *34*, 2255−2260.

(11) Huheey, J. E.; Keiter, E. A.; Keiter, R. L.; Medhi, O. K. *Inorganic Chemistry: Principles of Structure and Reactivity;* Pearson Education: Upper Saddle River, NJ, 2006.

(12) Selected reviews: (a) Bauer, I.; Knölker, H.-J. *Chem. Rev.* **2015**, *115*, 3170−3387. (b) Riener, K.; Haslinger, S.; Raba, A.; Hogerl, M. P.; Cokoja, M.; Herrmann, W. A.; Kühn, F. E. *Chem. Rev.* **2014**, *114*, 5215−5272. (c) Enthaler, S.; Junge, K.; Beller, M. *Angew. Chem., Int. Ed.* **2008**, *47*, 3317−3321. (d) Bolm, C.; Legros, J.; Le Paih, J.; Zani, L. *Chem. Rev.* **2004**, *104*, 6217−6254. Selected examples of diphosphine iron catalysts: (e) Asako, S.; Ilies, L.; Nakamura, E. *J. Am. Chem. Soc.* **2013**, *135*, 17755−17757. (f) Hatakeyama, T.; Okada, Y.; Yoshimoto, Y.; Nakamura, M. *Angew. Chem., Int. Ed.* **2011**, *50*, 10973−10976. (g) Hatakeyama, T.; Hashimoto, T.; Kondo, Y.; Fujiwara, Y.; Seike, H.; Takaya, H.; Tamada, Y.; Ono, T.; Nakamura, M. *J. Am. Chem. Soc.* **2010**, *132*, 10674−10676.

(13) For reviews see: (a) Boudier, A.; Breuil, P.-A. R.; Magna, L.; Olivier-Bourbigou, H.; Braunstein, P. *Chem. Commun.* **2014**, *50*, 1398−1407. (b) Bianchini, C.; Giambastiani, G.; Rios, I. G.; Mantovani, G.; Meli, A.; Segarra, A. M. *Coord. Chem. Rev.* **2006**, *250*, 1391−1418.

(14) Selected examples: (a) Zhang, W.; Sun, W.-H.; Redshaw, C. *Dalton Trans.* **2013**, *42*, 8988−8997. (b) Boudier, A.; Breuil, P.-A. R.; Magna, L.; Rangheard, C.; Ponthus, J.; Olivier-Bourbigou, H.; Braunstein, P. *Organometallics* **2011**, *30*, 2640−2642. (c) Appukuttan, V. K.; Liu, Y.; Son, B. C.; Ha, C.-S.; Suh, H.; Kim, I. *Organometallics* **2011**, *30*, 2285−2294. (d) Small, B. L.; Rios, R.; Fernandez, E. R.; Gerlach, D. L.; Halfen, J. A.; Carney, M. J. *Organometallics* **2010**, *29*, 6723−6731. (e) Kermagoret, A.; Tomicki, F.; Braunstein, P. *Dalton Trans.* **2008**, 2945−2955. (f) Sun, W.-H.; Hao, P.; Zhang, S.; Shi, Q.; Zuo, W.; Tang, X.; Lu, X. *Organometallics* **2007**, *26*, 2720−2734. (g) Small, B. L.; Rios, R.; Fernandez, E. R.; Carney, M. J. *Organometallics* **2007**, *26*, 1744−1749. (h) Bianchini, C.; Giambastiani, G.; Rios, I. G.; Meli, A.; Oberhauser, W.; Sorace, L.; Toti, A. *Organometallics* **2007**, *26*, 5066−5078. (i) Sun, W.-H.; Jie, S. Y.; Zhang, S.; Zhang, W.; Song, Y. X.; Ma, H. W. *Organometallics* **2006**, *25*, 666−677. (j) Speiser, F.; Braunstein, P.; Saussine, L. *Dalton Trans.* **2004**, 1539−1545. (k) Cowdell, R.; Davies, C. J.; Hilton, S. J.; Marechal, J. D.; Solan, G. A.; Thomas, O.; Fawcett, J. *Dalton Trans.* **2004**, 3231−3240. (l) Bianchini, C.; Giambastiani, G.; Guerrero, I. R.; Meli, A.; Passaglia, E.; Gragnoli, T. *Organometallics* **2004**, *23*, 6087−6089. (m) Chen, Y. F.; Qian, C. T.; Sun, J. *Organometallics* **2003**, *22*, 1231−1236. (n) Chen, Y. F.; Chen, R. F.; Qian, C. T.; Dong, X. C.; Sun, J. *Organometallics* **2003**, *22*, 4312−4321. (o) Britovsek, G. J. P.; Gibson, V. C.; Kimberley, B. S.; Mastroianni, S.; Redshaw, C.; Solan, G. A.; White, A. J. P.; Williams, D. J. *J. Chem. Soc., Dalton Trans.* **2001**, 1639−1644. (p) Small, B. L.; Brookhart, M. *J. Am. Chem. Soc.* **1998**, *120*, 7143−7144.

(15) For recent reviews see: (a) Poli, R.; Allan, L. E. N.; Shaver, M. P. *Prog. Polym. Sci.* **2014**, *39*, 1827−1845. (b) Riener, K.; Haslinger, S.; Raba, A.; Högerl, M. P.; Cokoja, M.; Herrmann, W. A.; Kühn, F. E. *Chem. Rev.* **2014**, *114*, 5215−5272. Selected examples: (c) Shaver, M. P.; Allan, L. E. N.; Rzepa, H. S.; Gibson, V. C. *Angew. Chem., Int. Ed.* **2006**, *45*, 1241−1244. (d) Gibson, V. C.; O'Reilly, R. K.; Wass, D. F.; White, A. J. P.; Williams, D. J. *Macromolecules* **2003**, *36*, 2591−2593. (e) Gibson, V. C.; O'Reilly, R. K.; Reed, W.; Wass, D. F.; White, A. J. P.; Williams, D. J. *Chem. Commun.* **2002**, 1850−1851. (f) Ando, T.; Kamigaito, M.; Sawamoto, M. *Macromolecules* **1997**, *30*, 4507−4510.

(16) (a) Layfield, R. A. *Organometallics* **2014**, *33*, 1084−1099. (b) Danopoulos, A. A.; Braunstein, P.; Wesolek, M.; Monakhov, K.; Yu; Rabu, P.; Robert, V. *Organometallics* **2012**, *31*, 4102−4105 and references therein.

(17) (a) Maithufi, N.; Otto, S. *Acta Crystallogr.* **2011**, *C67*, m279−m283. (b) Simón-Manso, E.; Valderrama, M. *J. Organomet. Chem.* **2006**, *691*, 380−386. (c) Zhang, Z.-Z.; Zhang, J.-K.; Zhang, W.-D.; Xi, H.-P.; Cheng, H.; Wang, H.-G. *J. Organomet. Chem.* **1996**, *515*, 1−9. (d) Harlan, C. J.; Wright, T. C.; Bott, S. G.; Atwood, J. L. *J. Crystallogr. Spectrosc. Res.* **1992**, *22*, 91−94. (e) Bell, S. E.; Field, J. S.; Haines, R. J. *J. Chem. Soc., Chem. Commun.* **1991**, 489−491. (f) Horsfield, E. C.; Engel, D. W.; Moodley, K. G. *Acta Crystallogr.* **1988**, *C44*, 80−82.

(18) (a) Li, C.-G.; Li, Y.-F.; Shang, J.-Y.; Lou, T.-J. *Transition Met. Chem.* **2014**, *39*, 373−378. (b) Song, L. C.; Li, Q. L.; Feng, Z. H.; Sun, X. J.; Xie, Z. J.; Song, H. B. *Dalton Trans.* **2013**, *42*, 1612−1626. (c) Ghosh, S.; Hogarth, G.; Hollingsworth, N.; Holt, K. B.; Richards, I.; Richmond, M. G.; Sanchez, B. E.; Unwin, D. *Dalton Trans.* **2013**, *42*, 6775−6792. (d) Wang, Y.; Li, Z.; Zeng, X.; Wang, X.; Zhan, C.; Liu, Y.; Zeng, X.; Luo, Q.; Liu, X. *New J. Chem.* **2009**, *33*, 1780−1789. (e) Song, L. C.; Li, C. G.; Ge, J. H.; Yang, Z. Y.; Wang, H. T.; Zhang,

DOI: 10.1021/acs.inorgchem.5b00834
Inorg. Chem. 2015, 54, 6547−6559

J.; Hu, Q. M. *J. Inorg. Biochem.* **2008**, *102*, 1973−1979. (f) Adam, F. I.; Hogarth, G.; Richards, I.; Sanchez, B. E. *Dalton Trans.* **2007**, 2495−2498.
(19) (a) Zhang, W.-H.; Chien, S. W.; Hor, T. S. A. *Coord. Chem. Rev.* **2011**, *255*, 1991−2024. (b) Braunstein, P. *J. Organomet. Chem.* **2004**, *689*, 3953−3967. (c) Braunstein, P.; Naud, F. *Angew. Chem., Int. Ed.* **2001**, *40*, 680−699. (d) Slone, C. S.; Weinberger, D. A.; Mirkin, C. A. *Prog. Inorg. Chem.* **1999**, *48*, 233−350.
(20) See, for example: Routaboul, L.; Braunstein, P.; Xiao, J.; Zhang, Z.; Dowben, P. A.; Dalmas, G.; Da Costa, V.; Félix, O.; Decher, G.; Rosa, L. G.; Doudin, B. *J. Am. Chem. Soc.* **2012**, *134*, 8494−8506.
(21) Langer, R.; Bönisch, F.; Maser, L.; Pietzonka, C.; Vondung, L.; Zimmermann, T. P. *Eur. J. Inorg. Chem.* **2015**, 141−148.
(22) Matouzenko, G. S.; Molnar, G.; Bréfuel, N.; Perrin, M.; Bousseksou, A.; Borshch, S. A. *Chem. Mater.* **2003**, *15*, 550−556.
(23) (a) Sun, C.-L.; Krause, H.; Fürstner, A. *Adv. Synth. Catal.* **2014**, *356*, 1281−1291. (b) Thomas, C. M.; Mankad, N. P.; Peters, J. C. *J. Am. Chem. Soc.* **2006**, *128*, 4956−4957. (c) Bianchini, C.; Dapporto, P.; Mealli, C.; Meli, A. *Inorg. Chem.* **1982**, *21*, 612−615.
(24) Cirera, J.; Ruiz, E.; Alvarez, S. *Inorg. Chem.* **2008**, *47*, 2871−2889.
(25) Casanova, D.; Cirera, J.; Llunell, M.; Alemany, P.; Avnir, D.; Alvarez, S. *J. Am. Chem. Soc.* **2004**, *126*, 1755−1763.
(26) Jabri, A.; Crewdson, P.; Gambarotta, S.; Korobkov, I.; Duchateau, R. *Organometallics* **2006**, *25*, 715−718.
(27) (a) Alvarez, S.; Ruiz, E. In *Supramolecular Chemistry, From Molecules to Nanomaterials;* Steed, J. W., Gale, P. A., Eds.; John Wiley & Sons: Chichester, U.K., 2012; Vol. *5*, pp 1993−2044. (b) Alvarez, S. *J. Am. Chem. Soc.* **2003**, *125*, 6795−6802.
(28) Aguilà, D.; Escribano, E.; Speed, S.; Talancón, D.; Yermán, L.; Alvarez, S. *Dalton Trans.* **2009**, 6610−6626.
(29) Diez, J.; Gamasa, M. P.; Gimeno, J.; Rodríguez, Y.; García-Granda, S. *Eur. J. Inorg. Chem.* **2004**, 2078−2085.
(30) Bóča, R. *Theoretical Foundations of Molecular Magnetism;* Elsevier: Amsterdam, The Netherlands,1999; p 293.
(31) Palamarciuc, T.; Oberg, J. C.; El Hallak, F.; Hirjibehedin, C. F.; Serri, M.; Heutz, S.; Létard, J.-F.; Rosa, P. *J. Mater. Chem.* **2012**, *22*, 9690−9695.
(32) Chilton, N. F.; Anderson, R. P.; Turner, L. D.; Soncini, A.; Murray, K. S. *J. Comput. Chem.* **2013**, *34*, 1164−1175.
(33) Bruker-Nonius. *Kappa CCD Reference Manual;* Nonius BV: The Netherlands, 1998.
(34) Sheldrick, G. M. *Acta Crystallogr.* **1990**, *A46*, 467−473.
(35) Sheldrick, G. M. *SHELXL-97, Program for crystal structure refinement;* University of Göttingen: Göttingen, Germany, 1997.
(36) Sheldrick, G. M. *Acta Cryst.* **2008**, *A64*, 112−122.
(37) Frisch, M. J.; et al. *Gaussian 09,* Revision A.1; Gaussian, Inc.: Wallingford, CT, 2009.
(38) Becke, A. D. *Phys. Rev. A* **1988**, *38*, 3098−3100.
(39) Perdew, J. P. *Phys. Rev. B* **1986**, *33*, 8822−8824.
(40) Schäfer, A.; Huber, C.; Ahlrichs, R. *J. Chem. Phys.* **1994**, *100*, 5829−5835.

DOI: 10.1021/acs.inorgchem.5b00834
Inorg. Chem. 2015, 54, 6547−6559